Multi-Physical Properties of Plasmonic Organic Solar Cells

Wallace C. H. Choy[*], Wei E. I. Sha, Xuanhua Li, and Di Zhang

(*Invited Paper*)

Abstract—Organic solar cells (OSCs) have recently attracted considerable research interest. For typical OSCs, it is highly desirable to have optically thick and physically thin thickness for strong light absorption and efficient carrier collection respectively. In the meantime, most organic semiconductors have short exciton diffusion length and low carrier mobility [1–3]. As a consequence, the active layers of OSCs are generally thin with a thickness of a few hundred nanometers to ensure the efficient extraction of carriers, hence limiting the total absorption of incident light. Optimizing both the optical and electrical (i.e., multi-physical) properties of OSCs is in demands for rationally designed device architectures. Plasmonic nanomaterials (e.g., metallic nanoparticles [4–6], nanorods [7, 8], nanoprisms [9, 10], etc.) have recently been introduced into different layers of multilayered solar cells to achieve highly efficient light harvesting. The multilayered solar cells structures commonly have active layer, carrier (electron and hole) transport layer and electrode (anode and cathode). Through the localized plasmonic resonances (LPRs) [11–16] from metallic nanomaterials, very strong near-fields will be generated, which can provide a large potential for enhancing optical absorption in the multilayered OSCs. Besides the optical effects, it has been reported that metallic nanomaterials can modify the morphology, interface properties as well as the electrical properties of OSCs which will significantly modify the performances of OSCs [17–23]. In this article, the effects of various optical resonance mechanisms and the theoretical studies of the multi-physical properties of OSCs will be reviewed. Meanwhile, the experimental optical and electrical effects of metallic nanomaterials incorporated in different layers of OSCs will be studied. The morphology and interface effects of metallic nanomaterials in the carrier transport layers on the performances of OSCs will also be described.

1. FUNDAMENTAL PHYSICS OF ORGANIC SOLAR CELLS WITH METALLIC NANOMATERIALS

1.1. Resonance Mechanisms and Couplings

Critically different from thin-film polycrystalline or amorphous silicon solar cells with active layer thicknesses of a few microns [24], the active layer of OSCs only has a few hundred nanometers or even thinner thickness [25–27]. Meanwhile, the refractive index of organic materials is typically low. The thin active layer with a low refractive index not only causes weak optical absorption, but also fundamentally limits (half-wavelength) the optical designs [11]. On one hand, a strong Fabry-Perot mode (or waveguide mode) cannot be supported. On the other hand, near-field concentration (rather than far-field scattering) will likely govern the optical design. We will describe versatile resonance mechanisms for enhancing the optical absorption of OSCs.

Fabry-Perot mode. Planar multilayer device structures support Fabry-Perot mode with a Lorentzian spectral line shape. Considering an incident plane wave, eigenmodes of the planar multilayer device

cannot be excited owing to momentum or phase mismatch. The Fabry-Perot mode is the mode coupling (overlap integral) between the excitation solution (with a plane wave source) and eigenmodes. The fundamental limit in the optical design of OSCs forbids the Fabry-Perot mode to be confined in a single active layer Thus, compared to thicker silicon solar cells, OSCs support weaker Fabry-Perot modes [28]. Importantly, non-planar device structures can support the Fabry-Perot mode because they can be approximately regarded as a superposition of different planar structures [29].

Quasi-guided mode. Space harmonics in periodic nanostructures offer the additional momentum for exciting the eigenmode or guided mode governed by the phase matching condition of $\mathrm{Re}(\beta) = k_0 \sin\theta + 2\pi m/P$, $m = 0, 1, 2$, etc. with a periodicity P and an incident angle θ of a typical 1D periodic structure. The complex propagation constant β suggests that the excited guided mode is not perfectly trapped but becomes a leaky wave. Arising from constructive and destructive interferences between a narrow discrete guided mode and a broad continuum (incident light), the quasi-guided mode [30] with an asymmetric and narrow Fano line shape has extraordinary transmittance and reflectance, which is also called Wood's anomaly [31, 32]. The pronounced quasi-guided mode enhances the optical absorption however, the enhancement is limited by the narrow bandwidth. Moreover most light energy will radiate away from the solar cell devices via the zero-order diffraction beam and light trapping only can be supported by high-order diffractions according to the total internal reflection. The supercell concept [33, 34] and double-interface gratings [35] can be employed to study the redistribution of the energy between diffraction beams of different orders.

Plasmonic modes. Excitation of plasmons by light induces a surface plasmonic resonance (SPR) for planar surfaces and LPR for nanometer-sized metallic structures [11–16]. SPRs are surface waves propagating at the interface between a dielectric and a metal, evanescently confined at the perpendicular direction. Using light to excite SPRs, the phase matching will be satisfied by using a periodic structure with space harmonics or a subscatterer generating evanescent waves. LPRs are non-propagating excitations of conduction electrons of a metallic nanomaterial coupled to electromagnetic fields. The curved surface of a metallic nanomaterial exerts an effective restoring force on the driven electrons, so that a resonance arises at a specific wavelength independent of wave vector. The half-wavelength limit in the optical design motivates researchers to focus on physical mechanisms of near-field concentration (not far-field scattering). Hence, plasmonic mode, which has unique features of near-field enhancement, is one of best candidates to boost the optical absorption of OSCs [36–41]. The resonant peaks of plasmonic modes strongly depend on the material, geometry, and surrounding environment and can be highly tunable and manipulated [4, 5, 9, 10, 42–45].

Mode Coupling/hybridization. The superradiant plasmonic mode oscillating in phase can be realized by the mode coupling and hybridization [46, 47], which occurs in the close-packed metallic nanomaterials. For example, longitudinal modes in a metallic nanosphere chain or symmetric modes in two coupled metallic plates increase the optical absorption of OSCs by several folds [43, 48]. Likewise, the LPR by a metallic nanosphere interacted with the SPR by a metallic plate leads to a coherent near-field enhancement [48, 49]. Furthermore, the plasmonic mode will couple to the Fabry-Perot mode through carefully optimizing both device and metallic structures [28, 38]. Finally, interferences between SPRs open up a plasmonic band gap and induce plasmonic band edges [44, 50–52]. Mode couplings and hybridizations offer an effective and flexible way in the optical design of OSCs.

Strong plasmonic-induced absorption enhancement. In order to achieve strong plasmonic-induced absorption enhancement, it is important to have a good spectral overlap between absorption regions of active materials and plasmonic resonances [53]. Importantly, in studying the spectral overlap, the plasmonic resonance in the device structure where the metal nanomaterials will be incorporated shall be determined because the plasmonic resonance will change depending on the optical environment [4, 44]. Besides, exploring mode hybridization is an alternative way to increase absorption enhancement. By tuning the thicknesses of active and spacer layers, plasmon-coupled Fabry-Perot mode can spectrally overlap with the absorption region of active materials [28, 34, 52]. Symmetry breaking and retardation effects allow us to excite dark modes or high-order modes of metallic nanomaterials with broadband and strong resonances [9, 10, 42, 54].

1.2. Theoretical Studies of Optical and Electrical Properties

The governing equations for describing optical properties of OSCs are Maxwell's equations

$$\nabla \times \mathbf{E} = -j\omega\mu_0\mathbf{H}, \quad \nabla \times \mathbf{H} = j\omega\varepsilon(\omega)\mathbf{E} \tag{1}$$

where $\mathbf{E}$ and $\mathbf{H}$ are electric and magnetic fields, and $\varepsilon(\omega)$ is the complex permittivity of materials. Computational electromagnetics [55], which is used for modeling the interaction of electromagnetic fields with objects and surrounding environment, plays an important role in characterizing and optimizing the optical design of OSCs. A rigorous, fast, and efficient solution to Maxwell's equations facilitates understanding device physics, reducing experimental costs, and shortening development periods. With the aid of state-of-the-art algorithms, important physical parameters in the optical design, such as optical absorption of active materials, can be extracted for analyzing and optimizing device structures. It is highly desirable to know the strengths and weaknesses of various theoretical methods for characterizing optical properties of OSCs.

Time-domain methods versus frequency-domain methods. Most optical materials are dispersive, therefore, a recursive convolution method [56] or a piecewise linear recursive convolution method [57] must be adopted for time-domain simulation [58, 59]. For metals with plasmonic effects in the visible light range, such as silver and gold, the complex refractive index has to be represented by a large number of terms in the Lorentz-Drude model [60] leading to a long calculation time. However, for frequency-domain methods, one can directly employ experimental refractive indices. Another challenge in time-domain methods is to treat periodic boundary conditions (in contrast to frequent-domain methods) for oblique incident waves [61]. In most places, unless a solar panel is mounted on an expensive tracking system, most of the time, light is incident on the array obliquely. Hence, the capability of frequency-domain methods to handle the case of oblique incidence is clearly an important advantage over time-domain methods. Meanwhile, time-domain methods have a concern in numerical dispersion and instability in contrast to frequency-domain methods [62, 63]. This drawback becomes more severe if a 3D large-scale OSC structure is investigated. A significant merit inherent from time-domain methods is a broadband simulation covering the whole solar spectrum of interest. The frequency-domain methods can employ parallel computing techniques to circumvent the problem.

Integral equation methods versus differential equation methods. Differential equation methods including finite-difference and finite-element algorithms [58, 59, 63, 64] handle a variety of inhomogeneous boundary conditions conveniently. The methods are suitable for modeling complicated device structures of OSCs incorporated with metallic nanostructures and nanomaterials. The generated matrix by differential equation methods is sparse matrix because of the 'local' differential operators of Maxwell's equations or wave equations. The methods consume a memory cost of O(N) and complexity of O(N) per matrix-vector multiplication by using Krylov subspace iteration algorithm [62, 65, 66]. Besides, multifrontal or multigrid methods [67, 68] can be used to accelerate the computation of the solution to differential equations. To model interactions between light and OSCs, an efficient absorption boundary condition, as well as additional volume grids enclosing the OSC device, shall be imposed.

In comparison with differential equation methods, integral equation methods [55, 62, 64] establish connections between field components and equivalent currents by using 'global' integral operators represented with the dyadic Green's functions. Consequently, integral equation methods have higher accuracy but produce full dense matrix. Matrix-free fast algorithms [55, 67, 69–75], such as fast Fourier transform and fast multipole methods, can considerably reduce computer resources (memory and CPU time) occupied by the dense matrix. Thanks to the Green's tensor, integral equation methods automatically satisfy the radiation boundary condition although it needs singularity treatments. Particularly, surface integral equation method (boundary element method) with a unique feature of surface triangulation has much less unknowns compared to volume integral equation method and differential equation methods. However, the surface integral equation method can only model a homogenous or piecewise-homogenous structure. Regarding a complex inhomogeneity in plasmonic OSCs with multiplayer device structures, the near-field computation by the surface integral equation method is hard to be implemented.

Mode-matching methods. Mode-matching method [76–79] is a commonly-adopted technique for modeling optical structures consisting of two or more separated regions. It is based on expanding the fields and matching them at the boundaries of different regions and thus lends itself naturally

to the analysis of multilayer optical devices. Most representatives of mode-matching methods involve rigorous coupled-wave analysis, scattering matrix method, and plane wave expansion method. Using few computer resources, these methods are very useful in studying optical responses of periodic-patterned OSC devices [80]. The zero-order and high-order transmittance and reflectance can be trivially obtained. However, mode-matching methods are not suited for characterizing plasmonic effects. On one hand, a large number of modes are required to capture plasmonic mode couplings resulting in a bad convergence. On the other hand, computing optical absorption of active materials for the OSCs incorporating metal nanostructures is difficult. The total absorbance (1-R-T) of OSC devices cannot correctly represent the optical absorption of active materials, and a postprocessing procedure is required for excluding the metallic absorption [43, 80]. Additionally, cascading many layer media with repeated matrix multiplications will lead to instability and bad accuracy, which always occurs in the OSCs with curved geometries.

Generation rate extraction. To model optical properties of OSCs with Maxwell's equations, the finite-difference frequency-domain method [29], integral equation with fast Fourier transform algorithm [48], and scattering matrix approach [80] can be used. After obtaining optical electric fields, the exciton generation rate G can be evaluated by

$$G(\mathbf{r}) = \int_{400}^{800} \frac{2\pi}{h} \varepsilon_0 n_r(\lambda) k_i(\lambda) |\mathbf{E}(\mathbf{r}, \lambda)|^2 \Gamma(\lambda) d\lambda \tag{2}$$

where n_r and k_r are the real and imaginary parts of refractive indices of active materials, h is the plank constant, and Γ is the AM 1.5G solar spectrum.

Optical and Electrical Properties Modeling. The performance of OSCs depends not only on photon harvesting but also on photocarrier transport. An electrical model is essential to understand full physics of OSCs. We have developed a unified finite-difference approach to characterize both optical and electrical (multiphysical) properties of OSCs. Figure 1 shows the schematic pattern of the multiphysical model.
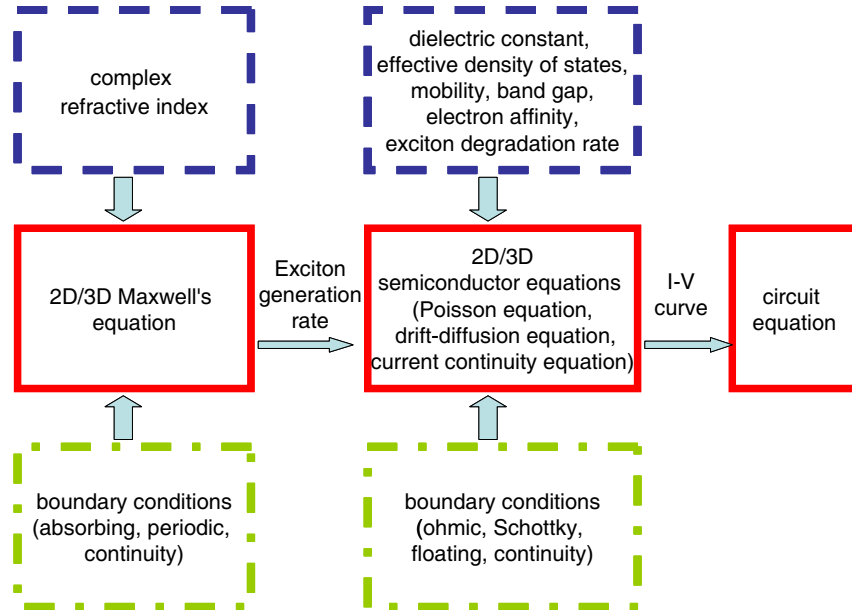
Figure 1. A multiphysics (optical and electrical) model for plasmonic OSCs.

Considering most polymers are strongly dispersive in the visible light range, the finite-difference frequency-domain method [29] can be adopted to discretize Maxwell's equations (See Equation (1)), the first-order differential operator can be approximated as

$$\frac{\partial f}{\partial x}\bigg|_i = \frac{f(i+1/2) - f(i-1/2)}{\Delta x} \tag{3}$$

The complex-coordinate stretched perfectly matched layer (PML) [81, 82] can be employed to absorb outgoing waves scattered from OSCs

$$\frac{\partial}{\partial \hat{x}} = \frac{1}{s_x}\frac{\partial}{\partial x}, \quad s_x = 1 - j\frac{\sigma(x)}{\omega \varepsilon_0} \tag{4}$$

where ε_o is the permittivity of free space, and σ is the conductivity of PML. Regarding 3D OSC devices with a 2D periodicity, Floquet-Bloch theorem can be used at the lateral sides of OSCs, i.e.,

$$\mathbf{E}(x + P_x, y + P_y, z) = \mathbf{E}(x, y, z) \exp(-jk_{x0}P_x) \exp(-jk_{y0}P_y) \tag{5}$$

where P_x and P_y are the periodicities along the x and y directions, respectively. k_{xo} and k_{yo} are the x and y components of wave numbers of the incident light, respectively.

For modeling photocarrier transport, recombination and collections in OSCs, three coupled nonlinear partial different equations (PDEs) including Poisson equation, drift-diffusion equation, and continuity equation [83–86] have to be solved.

$$\nabla \cdot (\varepsilon \nabla \phi) = -q(p - n) \tag{6}$$

$$\frac{\partial n}{\partial t} = \frac{1}{q}\nabla \cdot (q\mu_n n E_n + qD_n \nabla n) + QG - (1 - Q)R \tag{7}$$

$$\frac{\partial p}{\partial t} = -\frac{1}{q}\nabla \cdot (q\mu_p p E_p - qD_p \nabla p) + QG - (1 - Q)R \tag{8}$$

where q is the electron charge, ϕ is the potential, and n and p are electron and hole concentrations respectively. μ_n and μ_p are field-dependent mobility with the Frenkel-Poole form respectively for electrons and holes [87]. Moreover, D_n and D_p are diffusion coefficients of electrons and holes respectively, which can be accessed by the Einstein relations $D_{n,p} = \mu_{n,p}\frac{k_BT}{q}$. In addition, Q is the exciton dissociation probability expressed by the Onsager-Braun model [88, 89], R is the recombination rate with the Langevin bimolecular form [90], and G is the exciton generation rate obtained by the optical model (See Equation (2)). Particularly, the internal electrostatic fields considering extraction and injection barriers between carrier transport layers and the active layer are given by [23, 83]

$$E_n = -\nabla \phi - \frac{\nabla \chi}{q} - \frac{k_BT}{q}\nabla\left[\ln(N_c)\right] \tag{9}$$

$$E_p = -\nabla \phi - \frac{\nabla \chi}{q} - \frac{\nabla E_g}{q} + \frac{k_BT}{q}\nabla\left[\ln(N_v)\right] \tag{10}$$

where E_n and E_p are the internal electric fields for electrons and holes respectively, χ is the electron affinity, and E_g is the band gap. N_c and N_v are effective density of states (DOS) for electron and hole conducting materials, respectively. The extraction or injection barrier can be formed by the discontinuities of the electron affinity and effective DOS at the heterojunction interfaces between carrier transport layers and the active layer.

Boundary conditions are important to simulate electrical responses of OSCs. The potential boundary condition for the Schottky contact is [83]

$$\phi = V_{app} - \frac{W_m}{q} \tag{11}$$

where W_m is the work function of metal electrodes and V_{app} is the applied bias voltage. For the ohmic contact, the built-in potential relates to the difference between HOMO (highest occupied molecular orbital) and LUMO (lowest unoccupied molecular orbital) of carrier transport materials. The Neumann (floating) boundary condition is used to truncate the lateral sides of OSCs

$$\mathbf{n_v} \cdot \nabla \phi = 0 \tag{12}$$

where $\mathbf{n_v}$ is the unit vector normal to the non-electrode boundaries. Considering a finite surface recombination velocity and image force effect, the boundary conditions for currents at electrodes (organic-metal interfaces) shall adopt the Scott and Malliaras model [91]. Under infinite surface recombination velocity condition and ignoring the image force effect,

$$n = N_c \exp(-\phi_B^n/k_BT), \quad p = N_v \exp\left((-E_g + \phi_B^n)/k_BT\right) \text{ at cathode} \tag{13}$$

$$p = N_v \exp\left(-\phi_B^p/k_BT\right), \quad n = N_c \exp\left((-E_g + \phi_B^p)/k_BT\right) \text{ at anode} \tag{14}$$

where ϕ_B^n is the injection barrier between LUMO of the electron transport material and cathode, and ϕ_B^p is the injection barrier between HOMO of the hole transport material and anode.

For the space domain, we employed the Scharfetter-Gummel scheme [83, 86] to approximate the spatial differential operators. For the time domain, the semi-implicit strategy is utilized [83, 86]. For sparse matrix inversions, multifrontal fast solver was adopted [68]. Regarding algorithm details, please refer to our published works [23, 86, 92].

2. THE OPTICAL AND ELECTRICAL EFFECTS OF METAL NANOMATERIALS IN ACTIVE LAYERS

2.1. Optical Effects

Through various optical effects of nanomaterials such as LPR, scattering, etc. [39], it is possible to modify the light absorption of OSCs. There are many reports about incorporating metal nanomaterials into active layers to enhance light absorption in the OSCs [5, 8–10, 34, 42–44, 48, 93–113]. Active layer is a region which can absorb light and convert the absorbed light into charge carriers [114–116]. Generally, the materials, concentrations, shapes, sizes of the nanomaterials will strongly affect the optical effects [9, 39, 44, 109].

From materials point of view, the reports about embedding gold (Au) and silver (Ag) nanomaterials into active layer are popularly reported in recent years. Figures 2(a)–(c) show the results of Au
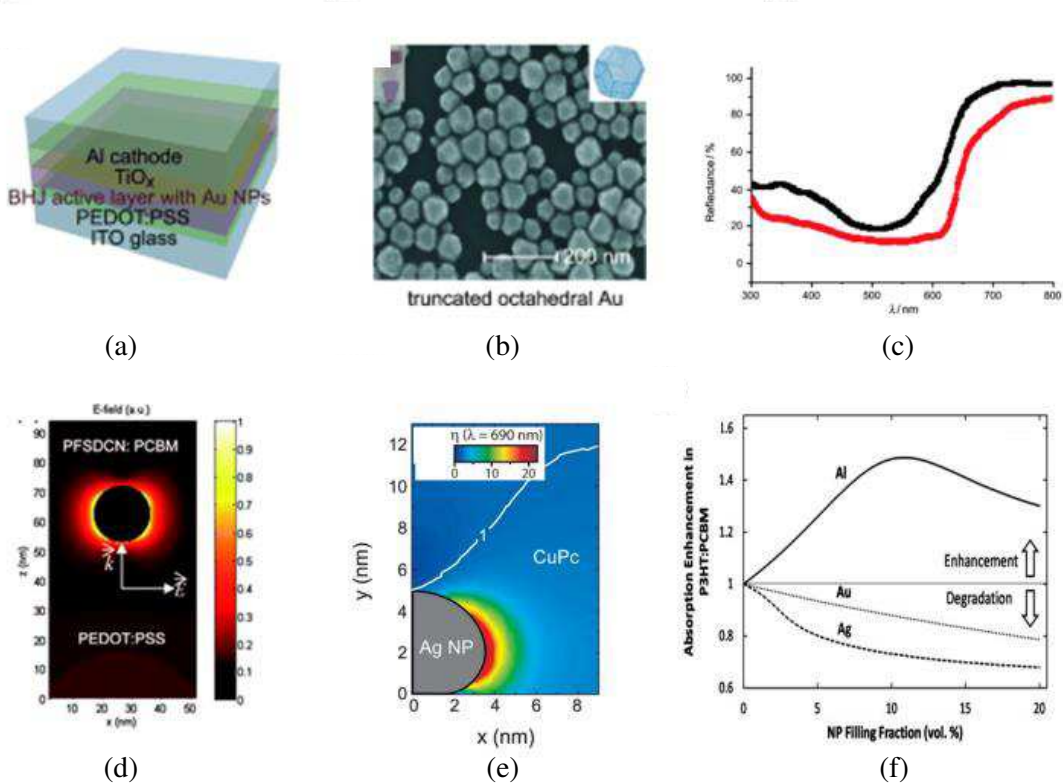
Figure 2. (a) Schematic of the OSC with incorporating Au nanoparticles, (b) SEM image of Au nanoparticles; inset of (b) is a schematic graph of Au nanoparticle, (c) experimental diffused reflection of the OSCs with (red line) or without (black line) incorporated Au nanoparticles into the active layer [109], (d) theoretical near field of Au nanoparticle when the Au nanoparticle with size of 18 nm is embedded into active layer [44], (e) theoretical contour-plot of $|E_{NP}|^2/|E_0|^2$, where E_{NP} and E_0 denote the E field with and without nanoparticles, respectively at wavelength of 690 nm [99], (f) theoretical absorption enhancement of different metal nanoparticles incorporated into the active layer of PCPDTBT: $PC_{70}BM$ [97].

nanoparticles incorporated into the active layer of poly(3-hexylthiophene) (P3HT):/[6,6]-phenyl C_{70} butyric acid methyl-ester ($PC_{70}BM$). As shown in Figure 2(c), the diffused reflectance spectra of the device fabricated with and without Au nanoparticles in $P3HT/PC_{70}BM$. The lower reflectivity of the device with Au nanoparticles indicates stronger absorption of the incident light. The improvement of absorption can be explained by the LPR effect and scattering of nanoparticles [109]. At the optimized blend ratio (5% Au nanoparticles), the short circuit current (J_{sc}) and power conversion efficiency (PCE) increase from $10.65\,\text{mA cm}^{-2}$ and 3.49% to $11.18\,\text{mA cm}^{-2}$ and 4.36%, respectively. Besides Au nanoparticles, Ag shows a most effectively optical trapping potential due to its relatively stronger scattering efficiency among noble metals in the visible range. In the report of Ref. [111], positive optical-trapping effects have been demonstrated through the addition of Ag nanoparticles with controlled diameter size in active layer. The optical effects of Au nanoparticles incorporated into the active layer of OSCs with other donor polymers such as poly[2,7-(9,9-dioctylfluorene)-alt-2-((4-(diphenylamino)phenyl)thiophen-2-yl)malononitrile] (PFSDCN) are also investigated in detail [44]. The work shows that LSPR excited by the metal nanoparticles can enhance the light absorption in the active layer of OSCs because the strong near field mainly distributes laterally along the active layer as described in Figure 2(d). Besides, the near-field interactions between Ag nanoparticle surface plasmons and small molecules excitons in thin-films have been studied. As shown in Figure 2(e), very large field enhancement close to the Ag nanoparticles (NPs) surface has also been observed like the case shown in Figure 2(d), which will contribute to the absorption enhancement. In addition, the near-field plasmon-exciton interactions between Ag NPs and organic molecules in thin-film have been probed experimentally by time-averaged and time-resolved photoluminescence (PL) measurement, which are used to determine the distance dependence of the plasmon-exciton interaction when a transparent, non-emitting spacer layer between the organic emitter and the Ag NPs is applied [99, 117]. Besides, large AuAg alloy nanoparticles have been introduced in organic media using a one-plot reaction and enhance the PCE of OSCs by taking advantage of plasmonic light-trapping effect [118]. Theoretically, it is found that Al nanoparticles yield significantly greater enhancement than Ag or Au nanoparticles because much higher plasma frequency of Al nanoparticles ensures a better overlap between plasmon resonance and absorption band of OSCs (Figure 2(f)) [97]. Cu nanoparticles are also reported absorption and current enhancement [106]. Although metals such as Al, Cu are more low-cost in fabricating metal-enhanced OSCs, the synthesis of Al and Cu nanomaterials with well-controlled sizes and shapes and the concerns of oxidation need to be further investigated in the future.

The shape and size of metal nanomaterials (e.g., nanoparticles) are extensively demonstrated to show significant effect on the optical absorption [8, 9, 95, 110]. Earlier research on metal nanoparticles introduced into active layer focused on relatively small particles with diameter less than 10 nm. Although optically small nanoparticles create a very strong near field around the nanoparticles and enhance absorption of the active layer, too small nanoparticles embedded into active layer will partly decrease the PCE of OSCs mostly likely due to the large absorption loss portion in the extinction and quenching of the excited state in the polymer and segregation phenomena [107]. Relatively large metal nanoparticles (high order modes plasmonics contribute to scattering) can reflect and scatter more light and thereby increase the optical path length within the active layer [49, 109–111]. As shown in Figures 3(a) and (b), the absorption intensity of active layer gradually enhances as concentration of Au nanoparticles in the active layer increases. Especially, compared with small metal nanoparticles (20 nm diameter), a strong light-trapping ability is shown when relative large metal nanoparticles (50 nm diameter) are introduced (Figures 3(a) and (b)) [49].

Apart from the metal nanoparticles, other differently shaped nanomaterials are recently introduced into active layer for PCE enhancement. For example, Ag nanowires are demonstrated to improve absorption and PCE more effectively by addition into the active layer [95]. By comparing Ag nanowires with Ag nanoparticles, they find the Ag nanowire exhibits a stronger light-trapping ability (Figure 3(c)). In addition, Ag nanoplates embedded into OSCs also show obvious light-trapping effects compared that of Ag nanospheres [110]. Meanwhile, triangular Ag nanoprisms show many interesting properties including large electromagnetic field enhancement particularly at the nanoprism corners, broad tunability of their plasmon resonances across the visible spectrum, and self-assembly without aggregation due to the surfactant on nanoprism in the active layer [119]. By incorporating Ag nanoprisms into P3HT:PCBM active layer and further studying the surface plasmon Raman spectrum
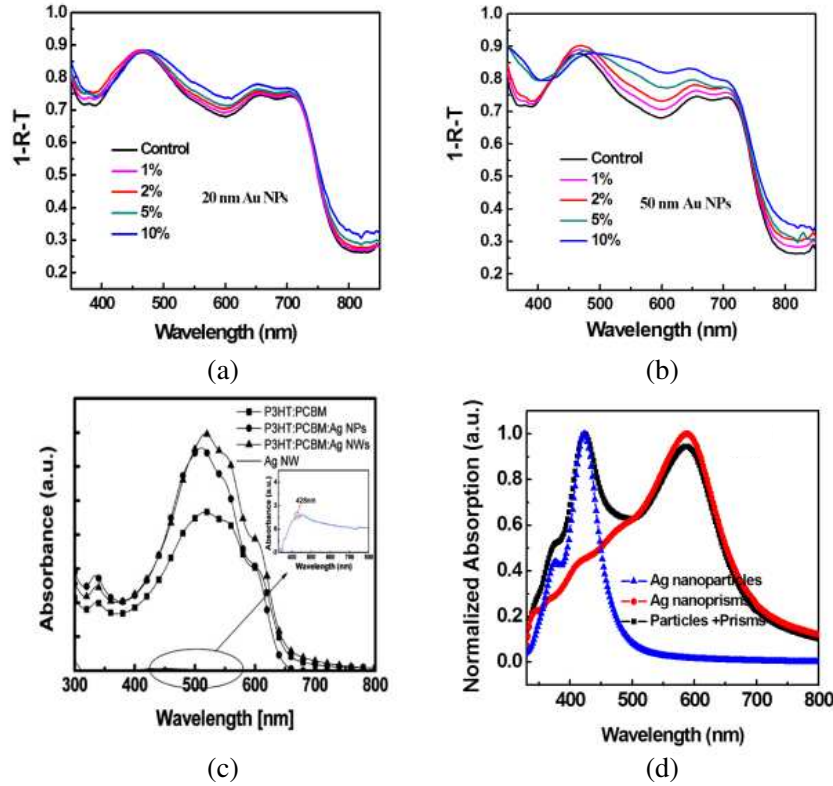
Figure 3. Extracted absorption (1-diffused reflection-transmission) of active layer with incorporated different sized metal nanoparticles: (a) 20 nm Ag nanoparticle, (b) 50 nm Ag nanoparticle [49], (c) absorption of the active layer with incorporated different shaped metal nanomaterials. Inset of Figure 3(c) is the absorption of Ag nanowire in water [95], (d) normalized absorption of active layer with incorporated different shaped nanomaterials [9].

(SERS) to better study the plasmonic-enhanced OSCs [119], it is found that the Raman intensity of polymer (active layer) will be drastically enhanced if the plasmonic peak of the metal nanomaterials incorporated into the active layer matches well with the laser wavelength of the Raman instrument. In order to provide an electrically insulating surface that does not interfere with carrier generation and transport inside the active layer, some work introduce silica-coated Ag or Au nanospheres into the active layer for high performance OSCs [8, 93]. Most of these studies show that the shape of the metal nanomaterials is a critical factor in maximizing the light scattering and trapping in OSCs.

The resonant wavelength region of metal nanomaterials is typically narrow, determined by the nanomaterials size, shape, and its local dielectric environment, which inevitably limits the PCE enhancement to a narrow spectral range. Meanwhile, sunlight is a broadband light source. It is desirable to extend wavelength region of the enhanced light absorption by using plasmonic nanostructures. Recently, a new method based on combining differently shaped nanomaterials of Ag nanoparticles and Ag nanoprisms has been proposed and demonstrated to achieve broad spectral enhancement range (Figure 3(d)) [9]. The results demonstrated J_{sc} enhancements of 17.91%, PCE enhancement of 19.44% as compared to pre-optimized control OSCs.

2.2. Electrical Effects

Regarding the electrical effects of the metal nanomaterials on OSCs, the metal nanomaterials can improve the charge carrier transport in the active layer. An early report of nanoparticles incorporated in active layer has stated that the increase of solar cell performance may be due to the introduction of dopant states which increase the electrical conductivity of the active layer [96]. Recently, incorporation

of Ag nanowire into the active layer of OSCs has been shown to increase both hole and electron mobility. Through the time-of-flight method for measuring mobility, it is reported that the active layer film has a 1.5 times larger electron mobility/hole mobility after the introduction of Ag nanowires into the active layer. As a result, an improved PCE has been observed [95]. Importantly, it is found that the increased hole mobility and better balance of electron and hole mobilities can be
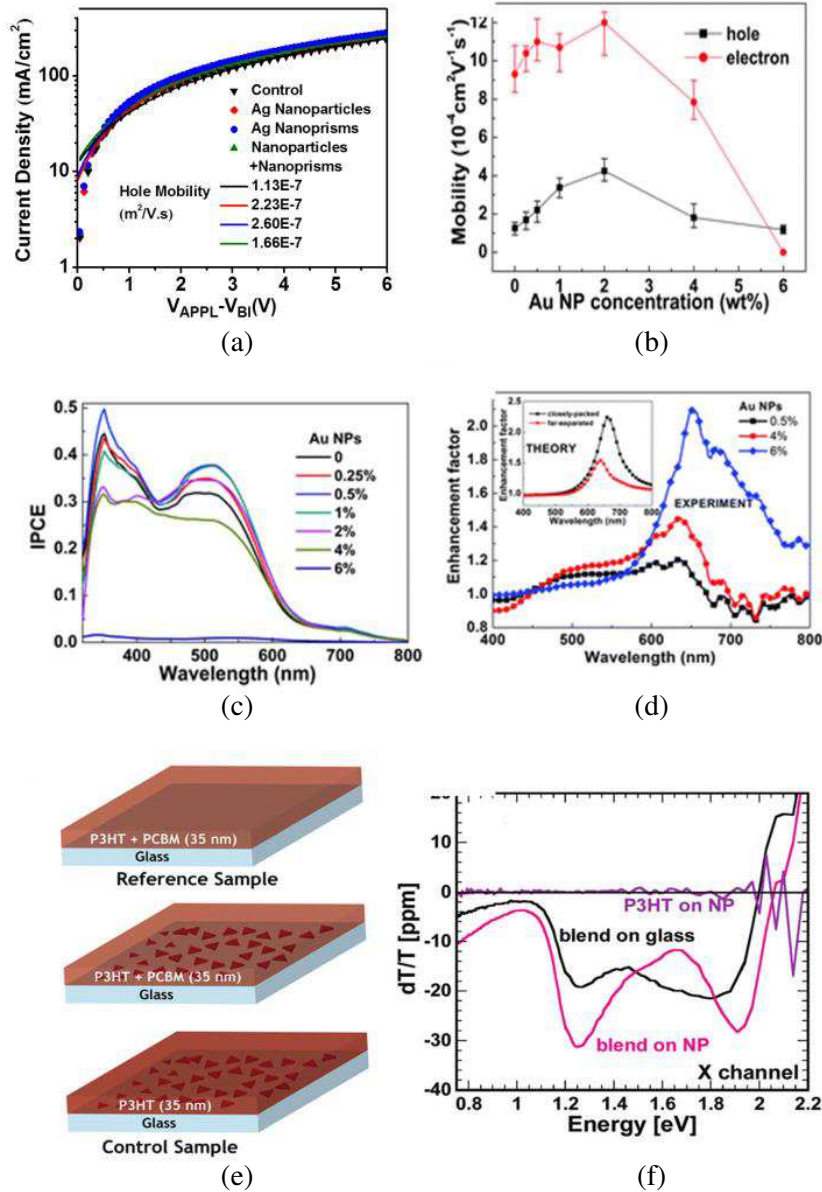
Figure 4. (a) Hole-only device with and without metal nanomaterials [9], (b) Au nanoparticle concentration effect on the mobility in the OSCs, (c) Au nanoparticles concentration effect on incident photon to current efficiency (IPCE) of OSCs with or without embedded metal nanoparticles into OSCs, and (d) Au nanoparticles concentration effect on the absorption of device with or without embedded metal nanoparticles into OSCs. Inset of Figure 4(d) is the theory study on concentration effect on the absorption of device with or without embedded metal nanoparticles into OSCs [44], (e) schematic of three different samples for photoinduced absorption spectroscopy measurements using KNP-525 silver nanoprisms, and (f) in-phase (X-channel) photoinduced absorption spectroscopy spectra for the two blend samples and the control sample using a blue pump (455 nm) LED [10].

achieved when incorporating Au or Ag nanomaterials into active layer, which can partly account for the increased J_{sc} and the higher fill factor (FF) [5, 9, 49]. The FF is defined as the ratio of the maximum output power to the product of the J_{sc} and open circuit voltage (V_{OC}), which is a key parameter in characterizing solar cell performance. As shown in Figure 4(a), the hole mobility improves from $1.14 \cdot 10^{-7}\,\mathrm{m^2 V^{-1} s^{-1}}$ (control) to $2.23 \cdot 10^{-7}\,\mathrm{m^2 V^{-1} s^{-1}}$ (with Ag nanoparticles), $2.60E \cdot 10^{-7}\,\mathrm{m^2 V^{-1} s^{-1}}$ (Ag nanoprisms), and $2.60 \cdot 10^{-7}\,\mathrm{m^2 V^{-1} s^{-1}}$ (Ag nanoparticles + nanoprisms), determined by the space-charge-limited current (SCLC) model together with hole-dominated devices with structures of ITO/poly-(3,4-ethylenedioxythiophene): poly(styrenesulfonate) (PEDOT:PSS) (30 nm)/P3HT:PCBM (220 nm) with and without Ag nanomaterials/MoO$_3$ (15 nm)/Ag [9].

In addition, the carrier mobilities are also affected by the concentration of metal nanoparticles doped into the active layer [44]. As shown in Figures 4(b)–(d), at high concentration compared to optimized concentration, the carrier mobility is expected to be degraded (Figure 4(b)); and then OSCs will encounter deterioration of device performances (Figure 4(d)) although the absorption of OSCs continuously increases to higher value (Figure 4(c)). It is also reported that the concentration of metal nanoparticles in the active layer is proportional to the optical absorption enhancement of active layer but will produce partially different electrical effect, such as decreased V_{oc} and FF [109–111]. Therefore, it is very important to carefully tune the concentration of metal nanoparticles for achieving metal-enhance organic solar cells.

Besides affecting carrier mobilities, the metal nanomaterials incorporating into the active layer will produce positive effect on photogeneration rate. Very recently, Ginger et al. have reported a plasmon-enhanced charge carrier generation in organic photovoltaic films using silver nanoprisms by photoinduced absorption spectroscopy, which provides a new route to metal-enhanced organic solar cells (Figures 4(e) and (f)) [10]. In general, reports about enhancing PCE by dispersing metal nanoparticles in the active layer of OSCs are very popular and the corresponding effects and roles including improving optical and electrical properties have already sufficiently revealed.

3. THE OPTICAL AND ELECTRICAL EFFECTS OF METAL NANOMATERIALS IN CARRIER TRANSPORT LAYERS

3.1. Optical Effects

Light trapping is an important strategy for thin-film OSCs to improve light absorption and thus the device performance [49, 120, 121]. Enabled by LPRs, metallic nanomaterials embedded in the active layer have been extensively studied for improving the light absorption of OSCs as described in previous section. Nevertheless, when the metallic nanomaterials are incorporated into the interface layer, it is a matter for debate whether the improved performance of OSCs is mainly due to the direct optical enhancement in the light absorption of OSC devices.

It is reported that the incorporation of plasmonic Ag nanoparticles (with a size of $\sim 13\,\mathrm{nm}$) between the surface modified electrode and the PEDOT:PSS hole transporting layer [17]. The authors attribute the increased PCE of the NP-embedded OSCs mainly to the improved photocurrent density as a result of enhanced absorption of the photoactive conjugate polymer. Meanwhile, Au nanoparticles with size of 70–80 nm have been added into the interconnecting layer of PEDOT:PSS in an inverted plasmonic polymer tandem solar cell [6]. The authors demonstrated simultaneous enhancement in efficiencies of both the top and bottom subcells. The improvement is ascribed to the enhanced optical absorption from the Au NPs without degrading the electrical characteristics within the tandem cell as shown in Figure 5(a). For the large Au NPs, high-order quadrupole distribution of the near-field can be obtained. In two other different studies, the enhanced performance of OSCs using nanoparticle blended PEDOT:PSS layer are also observed [122, 123]. Besides improved optical absorption, the enhancement is also from the increase of the probability of exciton dissociation. Differently, some theoretical and experimental results rule out direct optical effects from Au NPs doped in the PEDOT:PSS layer within OSC devices particularly for Au NPs with size smaller than thickness of the carrier transport layer, as there is no clear light absorption enhancement observed in the active layer as shown in Figure 5(b) [4]. Theoretical modeling conducted by the authors indicates that the very strong near field around Au NPs from the dipole resonance of LPRs mainly distributes laterally along the PEDOT:PSS layer rather than vertically into the adjacent active layer as shown in Figure 5(c). As a result, only relatively small optical
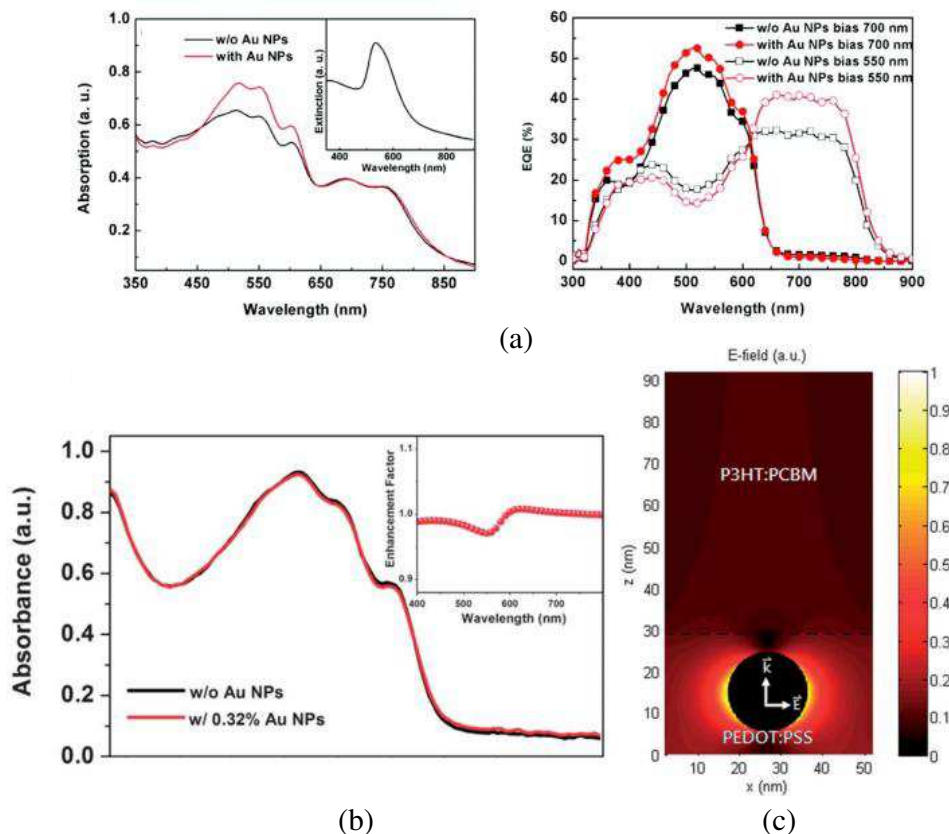
Figure 5. (a) Comparison of tandem cells results with and without Au NPs in the PEDOT:PSS layer: (left) absorption of the tandem solar cell (inset shows extinction spectrum of Au solution), and (right) external quantum efficiency of the tandem solar cell [6]; (b) absorbance of the PEDOT:PSS/P3HT:PCBM film with or without Au NP incorporation (0.32 wt%), with inset showing theoretical absorption enhancement factor [4]; (c) theoretical electric field profile in the PEDOT:PSS:Au NPs/P3HT:PCBM PSCs [4].

enhancement can be obtained. Further investigation reveals the underlying origin for the enhanced OSC performance to be the electrical and morphological changes introduced by the metallic NPs, i.e., reduced PEDOT:PSS resistance, increased interfacial roughness which contributes to the improvement of hole collection efficiency and reduced exciton quenching.

3.2. Material Effects of Metallic Nanomaterials for Interface Modification

Besides the potential optical enhancement, the material effects of the nanoscale metal are very interesting aspects of the metallic nanomaterials which are equally important for improving the performance of OSCs. When incorporated at the interface, the metallic nanomaterials can have a series of material effects on the properties of OSCs such as electrical characteristics, interface morphology, energy alignment and surface wettability. Commonly used interface layers such as PEDOT:PSS can be a problematic issue for the stability and performance of OSCs for several reasons. The aqueous PEDOT:PSS suspensions are strongly acidic (pH $\sim$ 1) [124] and can potentially introduce water into the active layer [125]. In this regard, metallic nanomaterials incorporated between the active layer and the electrodes can provide PEDOT-free interface modifications with better energy aligning capabilities due to the wide selection range of materials and available treatments. It has been reported that an ultra-thin layer of metal nanoclusters at the anode can provide reduced energy barrier for hole collection, leading to improved performance in small molecule OSCs compared to the case without the nanoclusters [18, 19]. Moreover, a PEDOT-free approach was reported using UV-ozone (UVO) treated Au nanoclusters at
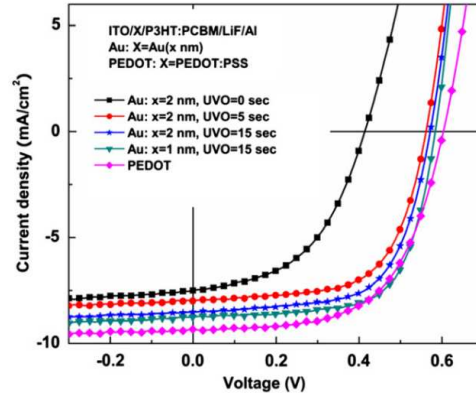
Figure 6. *J-V* characteristics of the representative OSCs using UVO treated Au nanoclusters and reference PEDOT layer [20].

Table 1. Performance of the OSCs using different UVO treated Au nanoclusters. The device structure is ITO/Au (x nm)/P3HT:PCBM/LiF/Al, and the structure of the conventional PEDOT-based PSC is ITO/PEDOT:PSS/P3HT:PCBM/LiF/Al [20].

Au thickness: x (nm)	J_{SC} (mA/cm^2)	V_{OC} (V)	FF (%)	PCE (%)	R_S (Ω cm^2)
0	8.33	0.52	55.9	2.42	2.8
1	8.75	0.59	67.2	3.47	1.8
2	8.52	0.57	63.9	3.1	2
3	6.94	0.56	64.2	2.5	1.8
5	5.78	0.55	62.2	1.98	2.1
8	4.59	0.55	60	1.51	2.9
15	3.65	0.55	58	1.16	4.8
PEDOT-based	9.33	0.6	60.4	3.38	3.2

the anode interface in polymer solar cells as shown in Figure 6 [20]. The OSCs using the treated Au nanoclusters exhibited enhanced performance comparable to devices using PEDOT:PSS layer, while avoid stability issues arising from the PEDOT:PSS. The results showed that the UVO-treated Au offers favorable band alignment at the ITO/polymer interface for efficient hole collection, meanwhile reducing the series resistance as shown in Table 1.

More importantly, metallic nanomaterials have demonstrated potential applications as effective interface modifications for graphene electrode, which is a promising candidate for next generation flexible OSCs. Commonly used electrode materials such as indium tin oxide (ITO) have been reported with issues of being relatively expensive [126] chemically unstable [127] and brittle [128] which is not compatible with the flexible organic materials. On the other hand, the newly emerged graphene has competitive optical transparency [129] and electrical conductivity [130], while being potentially advantageous for low-cost and large-area production [131]. Furthermore, graphene electrode has been reported to be more mechanically robust and flexible than ITO, showing superior performance under bending [132–134]. By introducing a thin layer of Au nanoclusters on multi-layer graphene anode in OSC devices with shortened UVO treatment as shown in Figure 7(a) [21], graphene OSCs with enhanced FF and PCE are obtained, exhibiting better performance compared to graphene devices directly modified with PEDOT:PSS and UVO. Further analysis shows that the UVO treated Au nanoclusters considerably increase the work function of graphene anode to facilitate hole collection as shown in Figure 7(b). In addition, the improved interfacial contact and shortened UVO durations reduce the series resistance of OSCs significantly. In a more recent study, an Al-TiO$_2$ composite modified graphene cathode for OSCs was reported [22]. The evaporated Al nanoclusters in the composite benefit the graphene cathode
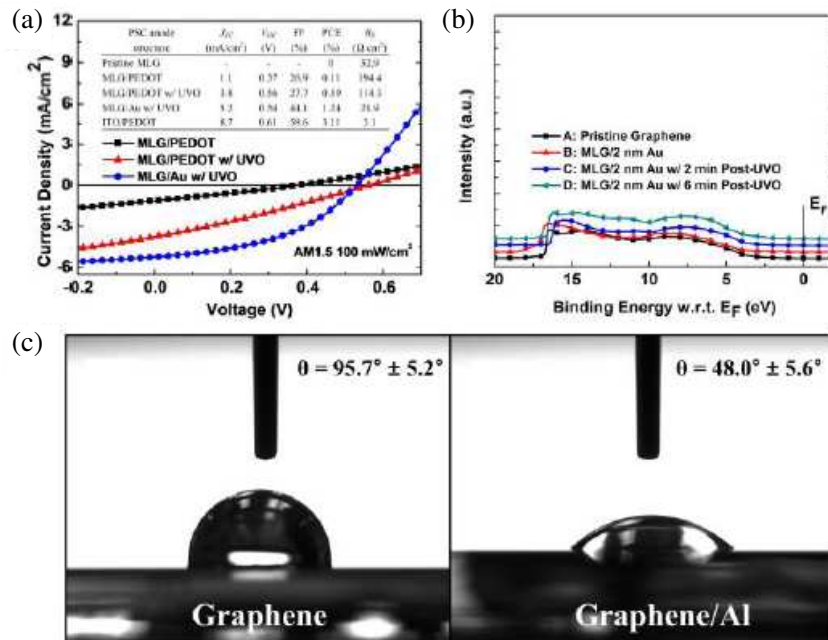
Figure 7. (a) Illuminated *J-V* characteristics of representative graphene OSCs using PEDOT and UVO treated Au nanocluster layer, inset summarizes the performance of respective graphene OSCs and reference ITO device [21]; (b) UPS spectra of graphene samples with different UVO treated Au nanocluster layers [21]; (c) surface contact angles of (left) graphene and (right) graphene/Al (~ 0.5 nm) samples [22].

by simultaneously achieving two roles, which are improving the surface wettability of graphene for subsequent TiO_2 deposition (see Figure 7(c)) and reducing its work function to offer better energy alignment. Consequently, the graphene cathode modified with Al-TiO_2 composite in inverted OSCs gave rise to one of the highest PCEs for graphene cathode OSCs (2.58%), reaching $\sim 75\%$ performance of control devices using ITO.

3.3. Plasmonic-electrical Effects of Metallic Nanomaterials for Enhanced Carrier Extraction

Previously, studies on the enhanced performance of OSCs generally focused on the individual effects from the optical and material aspects of the metallic nanomaterials, while it is quite interesting to investigate the changes in electrical properties directly induced by the optical plasmonic resonances in the semiconductor-metal (metallic nanomaterials) composite interface layer (hereafter named as the plasmonic-electrical effects) which can significantly improve the charge extraction in OSCs. UV light soaking is an interesting phenomenon observed in wide-bandgap semiconducting metal oxides such as TiO_2 and ZnO, where UV light is required to activate the carrier transport of the oxide layers. For TiO_2, the UV-excited electrons can fill the shallow electron traps in order to provide favorable electron extraction [135]. However, the required high-energy UV exposure for the metal oxide charge transport layers to become fully functional and efficient may degrade the organic materials in organic devices [136].

The use of metallic nanomaterials in metal oxide for photocatalytics and photoelectrochemistry applications has been previously reported [137–140]. Accordingly, under visible illumination with photon energy well below the UV region (near the plasmon resonance band of the metallic nanostructures), the presence of metallic nanostructures can lead to noticeable photocatalytic enhancements in the metal oxide layer. However, the physical mechanism of the enhancements remains inconclusive. Some studies suggest the injection of energetically active carriers (named as hot carriers) from the plasmonically excited Au/Ag NPs to TiO_2 to be responsible for the observed photocatalytic
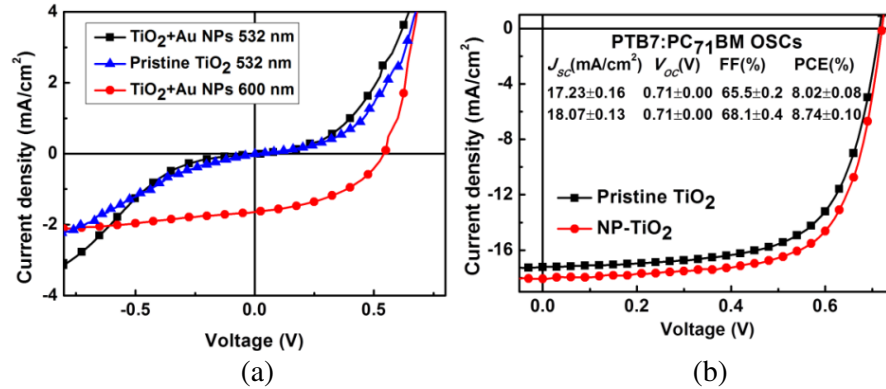
Figure 8. (a) *J-V* characteristics of P3HT:PC$_{61}$BM OSCs measured under monochromatic light of 532 nm and 600 nm with pristine TiO$_2$ and NPTiO$_2$ composite (TiO$_2$+Au NPs) as the electron transport layers (for pristine TiO$_2$ only *J-V* characteristics under 532 nm monochromatic light are shown) [23]; (b) representative AM1.5G *J-V* characteristics of inverted single-junction PTB7:PC$_{71}$BM OSCs with TiO$_2$ and NPTiO$_2$ composite (with the optimized NP concentration) as the electron transport layers; the device performances are summarized in the inset [23].

enhancement [137, 140, 141]. Meanwhile, some other studies report that such improvement of photocatalytic activity in the visible region is due to the local electric field enhancement near the TiO$_2$ surface, rather than by the direct transfer of charges between the metallic nanostructures and TiO$_2$ [138].

Recently, an efficient TiO$_2$ electron transport layer (ETL) for OSCs utilizing the plasmonic-electrical effects from metallic nanomaterials has been reported [23]. In the absence of Au NPs, OSCs using pristine TiO$_2$ ETL can only operate by UV activation with very short wavelength (< 400 nm), otherwise S-shape *J-V* characteristics are observed indicating poor device performance. On the other hand, OSCs using Au NPs incorporated TiO$_2$ is readily activated by a plasmonic wavelength (560–600 nm) which is far longer than the originally necessary UV light as shown in Figure 8(a). The performance of OSCs with different polymer active layers is further enhanced and an optimal efficiency of 8.74% is reached (see Figure 8(b)). Based on rigorously solving the Maxwell's equations and organic semiconductor equations an integrated optical and electrical model (i.e., a multiphysics model) as described in previously section is introduced in this work, which takes into account plasmonic-induced hot carrier tunneling probability and extraction barrier between TiO$_2$ and the active layer. Notably, both the theoretical and experimental results show that the contributions of metallic NPs in the oxide ETL of OSCs are the injection of plasmonically generated hot carriers into TiO$_2$. The hot carriers can fill the trap states in TiO$_2$ and therefore lower the effective extraction barrier. As a result, efficient carrier extraction in OSCs is introduced by this interesting mechanism facilitate.

4. CONCLUSIONS

In this article, we have summarized the effects of metallic nanomaterials on OSCs. The fundamental physics of various optical resonances and the approaches for modeling the optical and electrical properties of OSCs are described. By incorporating various metallic nanomaterials into the active layers, both the electrical and optical properties of OSCs will be modified. In addition, the shape, concentration and size of the metallic nanomaterials and the optical environment will also change the effects of the metallic nanomaterials for enhancing the performance of OSCs. For carrier transport layers, besides the optical and electrical effects, metallic nanomaterials will also change the interface properties including the wettability and worfunction. The interesting plamonic-electrical effects are also studied. Consequently, with the comprehensive understanding and appropriately introducing the multiphysical effects of metallic nanomaterials into various layers of OSCs, a new class of organic photovoltaics can be developed for emerging green energy applications.

ACKNOWLEDGMENT

REFERENCES

1. Shaw, P. E., A. Ruseckas, and I. D. W. Samuel, "Exciton diffusion measurements in poly(3-hexylthiophene)," *Advanced Materials*, Vol. 20, No. 18, 3516–3520, 2008.

2. Mcculloch, I., M. Heeney, C. Bailey, K. Genevicius, M. I. M. Shkunov, D. Sparrowe, S. Tierney, R. Wagner, W. M. Zhang, M. L. Chabinyc, R. J. Kline, M. D. Mcgehee, and M. F. Toney, "Liquid-crystalline semiconducting polymers with high charge-carrier mobility," *Nature Materials*, Vol. 5, No. 4, 328–333, 2006.

3. Zaumseil, J. and H. Sirringhaus, "Electron and ambipolar transport in organic field-effect transistors," *Chemical Reviews*, Vol. 107, No. 4, 1296–1323, 2007.

4. Fung, D. D. S., L. Qiao, W. C. H. Choy, C. Wang, E. Wei, F. Xie, and S. He, "Optical and electrical properties of efficiency enhanced polymer solar cells with Au nanoparticles in a PEDOT-PSS layer," *Journal of Materials Chemistry*, Vol. 21, No. 41, 16349–16356, 2011.

5. Xie, F. X., W. C. H. Choy, C. C. D. Wang, E. Wei, and D. D. S. Fung, "Improving the efficiency of polymer solar cells by incorporating gold nanoparticles into all polymer layers," *Applied Physics Letters*, Vol. 99, No. 153304, 2011.

6. Yang, J., J. You, C.-C. Chen, W.-C. Hsu, H.-R. Tan, X. W. Zhang, Z. Hong, and Y. Yang, "Plasmonic polymer tandem solar cell," *ACS Nano*, Vol. 5, No. 8, 6210–6217, 2011.

7. Lu, L. Y., Z. Q. Luo, T. Xu, and L. P. Yu, "Cooperative plasmonic effect of Ag and Au nanoparticles on enhancing performance of polymer solar cells," *Nano Letters*, Vol. 13, No. 1, 59–64, 2013.

8. Jankovic, V., Y. Yang, J. B. You, L. T. Dou, Y. S. Liu, P. Cheung, J. P. Chang, and Y. Yang, "Active layer-incorporated, spectrally tuned Au/SiO$_2$ core/shell nanorod-based light trapping for organic photovoltaics," *ACS Nano*, Vol. 7, No. 5, 3815–3822, 2013.

9. Li, X. H., W. C. H. Choy, H. F. Lu, W. E. I. Sha, and A. H. P. Ho, "Efficiency enhancement of organic solar cells by using shape-dependent broadband plasmonic absorption in metallic nanoparticles," *Advanced Functional Materials*, Vol. 23, No. 21, 2728–2735, 2013.

10. Kulkarni, A. P., K. M. Noone, K. Munechika, S. R. Guyer, and D. S. Ginger, "Plasmon-enhanced charge carrier generation in organic photovoltaic films using silver nanoprisms," *Nano Letters*, Vol. 10, No. 4, 1501–1505, 2010.

11. Gramotnev, D. K. and S. I. Bozhevolnyi, "Plasmonics beyond the diffraction limit," *Nature Photonics*, Vol. 4, No. 2, 83–91, 2010.

12. Barnes, W. L., A. Dereux, and T. W. Ebbesen, "Surface plasmon subwavelength optics," *Nature*, Vol. 424, No. 6950, 824–830, 2003.

13. Shalaev, V. M. and S. Kawata, *Nanophotonics with Surface Plasmons*, Elsevier, 2007.

14. Maier, S. A., *Plasmonics: Fundamentals and Applications*, Springer, 2007.

15. Giannini, V., A. I. Fernandez-Dominguez, Y. Sonnefraud, T. Roschuk, R. Fernandez-Garcia, and S. A. Maier, "Controlling light localization and light-matter interactions with nanoplasmonics," *Small*, Vol. 6, No. 22, 2498–2507, 2010.

16. Raether, H., *Surface Plasmons on Smooth and Rough Surfaces and on Gratings*, Springer-Verlag, Berlin, 1988.

17. Kim, S.-S., S.-I. Na, J. Jo, D.-Y. Kim, and Y.-C. Nah, "Plasmon enhanced performance of organic solar cells using electrodeposited Ag nanoparticles," *Applied Physics Letters*, Vol. 93, No. 7, 073303–073307, 2008.

18. Berredjem, Y., J. C. Bernède, S. Ouro Djobo, L. Cattin, M. Morsli, and A. Boulmokh, "On the improvement of the efficiency of organic photovoltaic cells by the presence of an ultra-thin metal layer at the interface organic/ITO," *The European Physical Journal — Applied Physics*, Vol. 44, No. 3, 223–228, 2008.

19. Kouskoussa, B., M. Morsli, K. Benchouk, G. Louarn, L. Cattin, A. Khelil, and J. C. Bernède, "On the improvement of the anode/organic material interface in organic solar cells by the presence of an ultra-thin gold layer," *Physica Status Solidi (A)*, Vol. 206, No. 2, 311–315, 2009.

20. Wang, C.-D. and W. C. H. Choy, "Efficient hole collection by introducing ultra-thin UV-ozone treated Au in polymer solar cells," *Solar Energy Materials and Solar Cells*, Vol. 95, No. 3, 904–908, 2011.

21. Zhang, D., W. C. H. Choy, C. C. D. Wang, X. Li, L. Fan, K. Wang, and H. Zhu, "Polymer solar cells with gold nanoclusters decorated multi-layer graphene as transparent electrode," *Applied Physics Letters*, Vol. 99, No. 22, 223302, 2011.

22. Zhang, D., F. Xie, P. Lin, and W. C. H. Choy, "Al-TiO$_2$ composite-modified single-layer graphene as an efficient transparent cathode for organic solar cells," *ACS Nano*, Vol. 7, No. 2, 1740–1747, 2013.

23. Zhang, D., W. C. H. Choy, F. Xie, W. E. I. Sha, X. Li, B. Ding, K. Zhang, F. Huang, and Y. Cao, "Plasmonic electrically functionalized TiO$_2$ for high-performance organic solar cells," *Advanced Functional Materials*, Vol. 23, No. 34, 4255–4261, 2013.

24. Chopra, K. L., P. D. Paulson, and V. Dutta, "Thin-film solar cells: An overview," *Progress in Photovoltaics*, Vol. 12, No. 2–3, 69–92, 2004.

25. Hoppe, H. and N. S. Sariciftci, "Organic solar cells: An overview," *Journal of Materials Research*, Vol. 19, No. 7, 1924–1945, 2004.

26. Brabec, C. J., S. Gowrisanker, J. J. M. Halls, D. Laird, S. J. Jia, and S. P. Williams, "Polymer-fullerene bulk-heterojunction solar cells," *Advanced Materials*, Vol. 22, No. 34, 3839–3856, 2010.

27. Deibel, C. and V. Dyakonov, "Polymer-fullerene bulk heterojunction solar cells," *Reports on Progress in Physics*, Vol. 73, No. 9, 096401, 2010.

28. Ferry, V. E., L. A. Sweatlock, D. Pacifici, and H. A. Atwater, "Plasmonic nanostructure design for efficient light coupling into solar cells," *Nano Letters*, Vol. 8, No. 12, 4391–4397, 2008.

29. Sha, W. E. I., W. C. H. Choy, and W. C. Chew, "A comprehensive study for the plasmonic thin-film solar cell with periodic structure," *Optics Express*, Vol. 18, No. 6, 5993–6007, 2010.

30. Tikhodeev, S. G., A. L. Yablonskii, E. A. Muljarov, N. A. Gippius, and T. Ishihara, "Quasiguided modes and optical properties of photonic crystal slabs," *Physical Review B*, Vol. 66, No. 4, 045102, 2002.

31. Luk'yanchuk, B., N. I. Zheludev, S. A. Maier, N. J. Halas, P. Nordlander, H. Giessen, and C. T. Chong, "The Fano resonance in plasmonic nanostructures and metamaterials," *Nature Materials*, Vol. 9, No. 9, 707–715, 2010.

32. Miroshnichenko, A. E., S. Flach, and Y. S. Kivshar, "Fano resonances in nanoscale structures," *Reviews of Modern Physics*, Vol. 82, No. 3, 2257–2298, 2010.

33. Martins, E. R., J. T. Li, Y. K. Liu, J. Y. Zhou, and T. F. Krauss, "Engineering gratings for light trapping in photovoltaics: The supercell concept," *Physical Review B*, Vol. 86, No. 4, 041404, 2012.

34. Chen, L. Z., W. C. H. Choy, and W. E. I. Sha, "Broadband absorption enhancement of organic solar cells with interstitial lattice patterned metal nanoparticles," *Applied Physics Letters*, Vol. 102, No. 25, 251112–251112-4, 2013.

35. Abass, A., K. Q. Le, A. Alu, M. Burgelman, and B. Maes, "Dual-interface gratings for broadband absorption enhancement in thin-film solar cells," *Physical Review B*, Vol. 85, No. 11, 115449, 2012.

36. Catchpole, K. R. and A. Polman, "Design principles for particle plasmon enhanced solar cells," *Applied Physics Letters*, Vol. 93, No. 19, 191113, 2008.

37. Mokkapati, S., F. J. Beck, A. Polman, and K. R. Catchpole, "Designing periodic arrays of metal nanoparticles for light-trapping applications in solar cells," *Applied Physics Letters*, Vol. 95, No. 5,

053115, 2009.

38. Pala, R. A., J. White, E. Barnard, J. Liu, and M. L. Brongersma, "Design of plasmonic thin-film solar cells with broadband absorption enhancements," *Advanced Materials*, Vol. 21, No. 34, 3504–3509, 2009.

39. Atwater, H. A. and A. Polman, "Plasmonics for improved photovoltaic devices," *Nature Materials*, Vol. 9, No. 3, 205–213, 2010.

40. Kang, M. G., T. Xu, H. J. Park, X. G. Luo, and L. J. Guo, "Efficiency enhancement of organic solar cells using transparent plasmonic Ag nanowire electrodes," *Advanced Materials*, Vol. 22, No. 39, 4378–4383, 2010.

41. Lee, J. Y. and P. Peumans, "The origin of enhanced optical absorption in solar cells with metal nanoparticles embedded in the active layer," *Optics Express*, Vol. 18, No. 10, 10078–10087, 2010.

42. Diukman, I., L. Tzabari, N. Berkovitch, N. Tessler, and M. Orenstein, "Controlling absorption enhancement in organic photovoltaic cells by patterning Au nano disks within the active layer," *Optics Express*, Vol. 19, No. 1, A64–A71, 2011.

43. Sha, W. E. I., W. C. H. Choy, Y. G. Liu, and W. C. Chew, "Near-field multiple scattering effects of plasmonic nanospheres embedded into thin-film organic solar cells," *Applied Physics Letters*, Vol. 99, No. 11, 113304, 2011.

44. Wang, C. C. D., W. C. H. Choy, C. Duan, D. D. S. Fung, W. E. I. Sha, F.-X. Xie, F. Huang, and Y. Cao, "Optical and electrical effects of gold nanoparticles in the active layer of polymer solar cells," *Journal of Materials Chemistry*, Vol. 22, No. 3, 1206–1211, 2012.

45. Bai, W. L., Q. Q. Gan, G. F. Song, L. H. Chen, Z. Kafafi, and F. Bartoli, "Broadband short-range surface plasmon structures for absorption enhancement in organic photovoltaics," *Optics Express*, Vol. 18, No. 23, A620–A630, 2010.

46. Prodan, E., C. Radloff, N. J. Halas, and P. Nordlander, "A hybridization model for the plasmon response of complex nanostructures," *Science*, Vol. 302, No. 5644, 419–422, 2003.

47. Nordlander, P., C. Oubre, E. Prodan, K. Li, and M. I. Stockman, "Plasmon hybridization in nanoparticle dimers," *Nano Letters*, Vol. 4, No. 5, 899–903, 2004.

48. Sha, W. E. I., W. C. H. Choy, Y. P. P. Chen, and W. C. Chew, "Optical design of organic solar cell with hybrid plasmonic system," *Optics Express*, Vol. 19, No. 17, 15908–15918, 2011.

49. Li, X., W. C. H. Choy, L. Huo, F. Xie, W. E. I. Sha, B. Ding, X. Guo, Y. Li, J. Hou, J. You, and Y. Yang, "Dual plasmonic nanostructures for high performance inverted organic solar cells," *Advanced Materials*, Vol. 24, No. 22, 3046–3052, 2012.

50. Bai, W. L., Q. Q. Gan, F. Bartoli, J. Zhang, L. K. Cai, Y. D. Huang, and G. F. Song, "Design of plasmonic back structures for efficiency enhancement of thin-film amorphous Si solar cells," *Optics Letters*, Vol. 34, No. 23, 3725–3727, 2009.

51. Min, C. J., J. Li, G. Veronis, J. Y. Lee, S. H. Fan, and P. Peumans, "Enhancement of optical absorption in thin-film organic solar cells through the excitation of plasmonic modes in metallic gratings," *Applied Physics Letters*, Vol. 96, No. 13, 133302, 2010.

52. Sha, W. E. I., W. C. H. Choy, and W. C. Chew, "Angular response of thin-film organic solar cells with periodic metal back nanostrips," *Optics Letters*, Vol. 36, No. 4, 478–480, 2011.

53. Khurgin, J. B., G. Sun, and R. A. Soref, "Practical limits of absorption enhancement near metal nanoparticles," *Applied Physics Letters*, Vol. 94, No. 7, 071103, 2009.

54. Akimov, Y. A., W. S. Koh, and K. Ostrikov, "Enhancement of optical absorption in thin-film solar cells through the excitation of higher-order nanoparticle plasmon modes," *Optics Express*, Vol. 17, No. 12, 10195–10205, 2009.

55. Chew, W. C. and J. M. Jin, *Fast and Efficient Algorithms in Computational Electromagnetics*, Artech House, Boston, 2001.

56. Luebbers, R., F. P. Hunsberger, K. S. Kunz, R. B. Standler, and M. Schneider, "A frequency-dependent finite-difference time-domain formulation for dispersive materials," *IEEE Transactions on Electromagnetic Compatibility*, Vol. 32, No. 3, 222–227, 1990.

57. Kelley, D. F. and R. J. Luebbers, "Piecewise linear recursive convolution for dispersive media using FDTD," *IEEE Transactions on Antennas and Propagation*, Vol. 44, No. 6, 792–797, 1996.

58. Sullivan, D. M., *Electromagnetic Simulation Using the FDTD Method*, Wiley-IEEE Press, New York, 2000.

59. Taflove, A. and S. C. Hagness, *Computational Electrodynamics: The Finite-difference Time-domain Method*, 3rd Edition, Artech House, Boston, 2005.

60. Veronis, G. and S. H. Fan, "Overview of simulation techniques for plasmonic devices," *Surface Plasmon Nanophotonics*, M. L. Brongersma and P. G. Kik, Eds., Springer, Dordrecht, Netherlands, 2007.

61. Veysoglu, M. E., R. T. Shin, and J. A. Kong, "A finite-difference time-domain analysis of wave scattering from periodic surfaces: Oblique-incidence case," *Journal of Electromagnetic Waves and Applications*, Vol. 7, No. 12, 1595–1607, 1993.

62. Chew, W. C., M. S. Tong, and B. Hu, *Integral Equation Methods for Electromagnetic and Elastic Waves*, Morgan & Claypool Publishers, 2009.

63. Jin, J. M., *The Finite Element Method in Electromagnetics*, Wiley-IEEE Press, New York, 1993.

64. Chew, W. C., *Waves and Fields in Inhomogenous Media*, Wiley-IEEE Press, New York, 1999.

65. Hestenes, M. R. and E. Stiefel, "Methods of conjugate gradients for solving linear systems," *Journal of Research of the National Bureau of Standards*, Vol. 49, No. 6, 409–436, 1952.

66. Vandervorst, H. A., "Bi-Cgstab — A fast and smoothly converging variant of Bi-Cg for the solution of nonsymmetric linear-systems," *Siam Journal on Scientific and Statistical Computing*, Vol. 13, No. 2, 631–644, 1992.

67. Chew, W. C., J. M. Jin, C. C. Lu, E. Michielssen, and J. M. M. Song, "Fast solution methods in electromagnetics," *IEEE Transactions on Antennas and Propagation*, Vol. 45, No. 3, 533–543, 1997.

68. Davis, T. A. and I. S. Duff, "An unsymmetric-pattern multifrontal method for sparse LU factorization," *Siam Journal on Matrix Analysis and Applications*, Vol. 18, No. 1, 140–158, 1997.

69. Greengard, L. and V. Rokhlin, "A fast algorithm for particle simulations," *Journal of Computational Physics*, Vol. 73, No. 2, 325–348, 1987.

70. Catedra, M. F., E. Gago, and L. Nuno, "A numerical scheme to obtain the RCS of 3-dimensional bodies of resonant size using the conjugate-gradient method and the fast fourier-transform," *IEEE Transactions on Antennas and Propagation*, Vol. 37, No. 5, 528–537, 1989.

71. Brandt, A., "Multilevel computations of integral-transforms and particle interactions with oscillatory Kernels," *Computer Physics Communications*, Vol. 65, No. 1–3, 24–38, 1991.

72. Draine, B. T. and P. J. Flatau, "Discrete-dipole approximation for scattering calculations," *Journal of the Optical Society of America A — Optics Image Science and Vision*, Vol. 11, No. 4, 1491–1499, 1994.

73. Phillips, J. R. and J. K. White, "A precorrected-FFT method for electrostatic analysis of complicated 3-D structures," *IEEE Transactions on Computer-aided Design of Integrated Circuits and Systems*, Vol. 16, No. 10, 1059–1072, 1997.

74. Song, J. M., C. C. Lu, and W. C. Chew, "Multilevel fast multipole algorithm for electromagnetic scattering by large complex objects," *IEEE Transactions on Antennas and Propagation*, Vol. 45, No. 10, 1488–1493, 1997.

75. Tsang, L., J. A. Kong, and K. H. Ding, *Scattering of Electromagnetic Waves: Theories and Applications*, Wiley, 2000.

76. Moharam, M. G., E. B. Grann, D. A. Pommet, and T. K. Gaylord, "Formulation for stable and efficient implementation of the rigorous coupled-wave analysis of binary gratings," *Journal of the Optical Society of America A — Optics Image Science and Vision*, Vol. 12, No. 5, 1068–1076, 1995.

77. Yonekura, J., M. Ikeda, and T. Baba, "Analysis of finite 2-D photonic crystals of columns and lightwave devices using the scattering matrix method," *Journal of Lightwave Technology*, Vol. 17, No. 8, 1500–1508, 1999.

78. Bienstman, P. and R. Baets, "Optical modelling of photonic crystals and VCSELs using eigenmode expansion and perfectly matched layers," *Optical and Quantum Electronics*, Vol. 33, No. 4–5, 327–341, 2001.

79. Johnson, S. G. and J. D. Joannopoulos, "Block-iterative frequency-domain methods for Maxwell's equations in a planewave basis," *Optics Express*, Vol. 8, No. 3, 173–190, 2001.

80. Chen, L. Z., W. E. I. Sha, and W. C. H. Choy, "Light harvesting improvement of organic solar cells with self-enhanced active layer designs," *Optics Express*, Vol. 20, No. 7, 8175–8185, 2012.

81. Chew, W. C. and W. H. Weedon, "A 3D perfectly matched medium from modified Maxwell's equations with stretched coordinates," *Microwave and Optical Technology Letters*, Vol. 7, No. 13, 599–604, 1994.

82. Berenger, J. P., "Three-dimensional perfectly matched layer for the absorption of electromagnetic waves," *Journal of Computational Physics*, Vol. 127, No. 2, 363–379, 1996.

83. Selberherr, S., *Analysis and Simulation of Semiconductor Devices*, Springer, 1984.

84. Koster, L. J. A., E. C. P. Smits, V. D. Mihailetchi, and P. W. M. Blom, "Device model for the operation of polymer/fullerene bulk heterojunction solar cells," *Physical Review B*, Vol. 72, No. 8, 085205, 2005.

85. Li, X. F., N. P. Hylton, V. Giannini, K. H. Lee, N. J. Ekins-Daukes, and S. A. Maier, "Bridging electromagnetic and carrier transport calculations for three-dimensional modelling of plasmonic solar cells," *Optics Express*, Vol. 19, No. 14, A888–A896, 2011.

86. Sha, W. E. I., W. C. H. Choy, Y. M. Wu, and W. C. Chew, "Optical and electrical study of organic solar cells with a 2D grating anode," *Optics Express*, Vol. 20, No. 3, 2572–2580, 2012.

87. Sievers, D. W., V. Shrotriya, and Y. Yang, "Modeling optical effects and thickness dependent current in polymer bulk-heterojunction solar cells," *Journal of Applied Physics*, Vol. 100, No. 11, 114509, 2006.

88. Onsager, L., "Initial recombination of ions," *Physical Review*, Vol. 54, No. 8, 554–557, 1938.

89. Braun, C. L., "Electric-field assisted dissociation of charge-transfer states as a mechanism of photocarrier production," *Journal of Chemical Physics*, Vol. 80, No. 9, 4157–4161, 1984.

90. Langevin, P., "Recombinaison et mobilites des ions dans les gaz," *Ann. Chim. Phys.*, Vol. 28, 433–530, 1903.

91. Scott, J. C. and G. G. Malliaras, "Charge injection and recombination at the metal-organic interface," *Chemical Physics Letters*, Vol. 299, No. 2, 115–119, 1999.

92. Sha, W. E. I., W. C. H. Choy, and W. C. Chew, "The roles of metallic rectangular-grating and planar anodes in the photocarrier generation and transport of organic solar cells," *Applied Physics Letters*, Vol. 101, No. 22, 223302, 2012.

93. Choi, H., J. P. Lee, S. J. Ko, J. W. Jung, H. Park, S. Yoo, O. Park, J. R. Jeong, S. Park, and J. Y. Kim, "Multipositional silica-coated silver nanoparticles for high-performance polymer solar cells," *Nano Letters*, Vol. 13, No. 5, 2204–2208, 2013.

94. Duche, D., P. Torchio, L. Escoubas, F. Monestier, J. J. Simon, F. Flory, and G. Mathian, "Improving light absorption in organic solar cells by plasmonic contribution," *Solar Energy Materials and Solar Cells*, Vol. 93, No. 8, 1377–1382, 2009.

95. Kim, C. H., S. H. Cha, S. C. Kim, M. Song, J. Lee, W. S. Shin, S. J. Moon, J. H. Bahng, N. A. Kotov, and S. H. Jin, "Silver nanowire embedded in P3HT:PCBM for high-efficiency hybrid photovoltaic device applications," *ACS Nano*, Vol. 5, No. 4, 3319–3325, 2011.

96. Kim, K. and D. L. Carroll, "Roles of Au and Ag nanoparticles in efficiency enhancement of poly(3-octylthiophene)/C-60 bulk heterojunction photovoltaic devices," *Applied Physics Letters*, Vol. 87, No. 20, 203113 (3 pages), 2005.

97. Kochergin, V., L. Neely, C. Y. Jao, and H. D. Robinson, "Aluminum plasmonic nanostructures for improved absorption in organic photovoltaic devices," *Applied Physics Letters*, Vol. 98, No. 13, 2011.

98. Naidu, B. V. K., J. S. Park, S. C. Kim, S. M. Park, E. J. Lee, K. J. Yoon, S. J. Lee, J. W. Lee, Y. S. Gal, and S. H. Jin, "Novel hybrid polymer photovoltaics made by generating

silver nanoparticles in polymer: Fullerene bulk-heterojunction structures," *Solar Energy Materials and Solar Cells*, Vol. 92, No. 4, 397–401, 2008.

99. Niesen, B., B. P. Rand, P. van Dorpe, D. Cheyns, H. Shen, B. Maes, and P. Heremans, "Near-field interactions between metal nanoparticle surface plasmons and molecular excitons in thin-films. Part I: Absorption," *The Journal of Physical Chemistry C*, Vol. 116, No. 45, 24206–24214, 2012.

100. Paci, B., A. Generosi, V. R. Albertini, G. D. Spyropoulos, E. Stratakis, and E. Kymakis, "Enhancement of photo/thermal stability of organic bulk heterojunction photovoltaic devices via gold nanoparticles doping of the active layer," *Nanoscale*, Vol. 4, No. 23, 7452–7459, 2012.

101. Paci, B., G. D. Spyropoulos, A. Generosi, D. Bailo, V. R. Albertini, E. Stratakis, and E. Kymakis, "Enhanced structural stability and performance durability of bulk heterojunction photovoltaic devices incorporating metallic nanoparticles," *Advanced Functional Materials*, Vol. 21, No. 18, 3573–3582, 2011.

102. Qu, D., F. Liu, Y. D. Huang, W. L. Xie, and Q. Xu, "Mechanism of optical absorption enhancement in thin film organic solar cells with plasmonic metal nanoparticles," *Optics Express*, Vol. 19, No. 24, 24795–24803, 2011.

103. Shen, H. H., P. Bienstman, and B. Maes, "Plasmonic absorption enhancement in organic solar cells with thin active layers," *Journal of Applied Physics*, Vol. 106, No. 7, 073109, 2009.

104. Spyropoulos, G. D., M. Stylianakis, E. Stratakis, and E. Kymakis, "Plasmonic organic photovoltaics doped with metal nanoparticles," *Photonics and Nanostructures-Fundamentals and Applications*, Vol. 9, No. 2, 184–189, 2011.

105. Spyropoulos, G. D., M. M. Stylianakis, E. Stratakis, and E. Kymakis, "Organic bulk heterojunction photovoltaic devices with surfactant-free Au nanoparticles embedded in the active layer," *Applied Physics Letters*, Vol. 100, No. 21, 213904, 2012.

106. Szeremeta, J., M. Nyk, A. Chyla, W. Strek, and M. Samoc, "Enhancement of photoconduction in a conjugated polymer through doping with copper nanoparticles," *Optical Materials*, Vol. 33, No. 9, 1372–1376, 2011.

107. Topp, K., H. Borchert, F. Johnen, A. V. Tune, M. Knipper, E. von Hauff, J. Parisi, and K. Al-Shamery, "Impact of the incorporation of Au nanoparticles into polymer/fullerene solar cells," *Journal of Physical Chemistry A*, Vol. 114, No. 11, 3981–3989, 2010.

108. Vedraine, S., P. Torchio, A. Merlen, J. Bagierek, F. Flory, A. Sangar, and L. Escoubas, "Optical characterization of organic blend films integrating metallic nanoparticles," *Solar Energy Materials and Solar Cells*, Vol. 102, No. 31–35, 2012.

109. Wang, D. H., D. Y. Kim, K. W. Choi, J. H. Seo, S. H. Im, J. H. Park, O. O. Park, and A. J. Heeger, "Enhancement of Donor-Acceptor polymer bulk heterojunction solar cell power conversion efficiencies by addition of Au nanoparticles," *Angewandte Chemie-International Edition*, Vol. 50, No. 24, 5519–5523, 2011.

110. Wang, D. H., J. K. Kim, G. H. Lim, K. H. Park, O. O. Park, B. Lim, and J. H. Park, "Enhanced light harvesting in bulk heterojunction photovoltaic devices with shape-controlled Ag nanomaterials: Ag nanoparticles versus Ag nanoplates," *Rsc Advances*, Vol. 2, No. 18, 7268–7272, 2012.

111. Wang, D. H., K. H. Park, J. H. Seo, J. Seifter, J. H. Jeon, J. K. Kim, J. H. Park, O. O. Park, and A. J. Heeger, "Enhanced power conversion efficiency in PCDTBT/PC70BM bulk heterojunction photovoltaic devices with embedded silver nanoparticle clusters," *Advanced Energy Materials*, Vol. 1, No. 5, 766–770, 2011.

112. Xue, M., L. Li, B. J. T. de Villers, H. J. Shen, J. F. Zhu, Z. B. Yu, A. Z. Stieg, Q. B. Pei, B. J. Schwartz, and K. L. Wang, "Charge-carrier dynamics in hybrid plasmonic organic solar cells with Ag nanoparticles," *Applied Physics Letters*, Vol. 98, No. 25, 253302, 2011.

113. Zhu, J. F., M. Xue, H. J. Shen, Z. Wu, S. Kim, J. J. Ho, A. Hassani-Afshar, B. Q. Zeng, and K. L. Wang, "Plasmonic effects for light concentration in organic photovoltaic thin films induced by hexagonal periodic metallic nanospheres," *Applied Physics Letters*, Vol. 98, No. 15, 151110, 2011.

114. Hiramoto, M., H. Fukusumi, and M. Yokoyama, "Organic solar-cell based on multistep charge separation system," *Applied Physics Letters*, Vol. 61, No. 21, 2580–2582, 1992.

115. Ma, T. L., "Progress in a new type of plastic organic solar cell," *Progress in Chemistry*, Vol. 18, No. 2–3, 176–181, 2006.

116. Takahashi, K., N. Kuraya, T. Yamaguchi, T. Komura, and K. Murata, "Three-layer organic solar cell with high-power conversion efficiency of 3.5%," *Solar Energy Materials and Solar Cells*, Vol. 61, No. 4, 403–416, 2000.

117. Niesen, B., B. P. Rand, P. van Dorpe, D. Cheyns, E. Fron, M. van der Auweraer, and P. Heremans, "Near-field interactions between metal nanoparticle surface plasmons and molecular excitons in thin-films. Part II: Emission," *Journal of Physical Chemistry C*, Vol. 116, No. 45, 24215–24223, 2012.

118. Chen, H. C., S. W. Chou, W. H. Tseng, I. Chen, P. Wen, C. C. Liu, C. Liu, C. L. Liu, C. H. Chen, and C. I. Wu, "Large AuAg alloy nanoparticles synthesized in organic media using a one-pot reaction: Their applications for high-performance bulk heterojunction solar cells," *Advanced Functional Materials*, Vol. 22, No. 19, 3975–3984, 2012.

119. Stavytska-Barba, M., M. Salvador, A. Kulkarni, D. S. Ginger, and A. M. Kelley, "Plasmonic enhancement of raman scattering from the organic solar cell material P3HT/PCBM by triangular silver nanoprisms," *The Journal of Physical Chemistry C*, Vol. 115, No. 42, 20788–20794, 2011.

120. Green, M. A. and S. Pillai, "Harnessing plasmonics for solar cells," *Nat. Photon.*, Vol. 6, No. 3, 130–132, 2012.

121. Wang, D. H., D. Y. Kim, K. W. Choi, J. H. Seo, S. H. Im, J. H. Park, O. O. Park, and A. J. Heeger, "Enhancement of Donor-Acceptor polymer bulk heterojunction solar cell power conversion efficiencies by addition of Au nanoparticles," *Angewandte Chemie International Edition*, Vol. 50, No. 24, 5519–5523, 2011.

122. Wu, J.-L., F.-C. Chen, Y.-S. Hsiao, F.-C. Chien, P. Chen, C.-H. Kuo, M. H. Huang, and C.-S. Hsu, "Surface plasmonic effects of metallic nanoparticles on the performance of polymer bulk heterojunction solar cells," *ACS Nano*, Vol. 5, No. 2, 959–967, 2011.

123. Chen, F.-C., J.-L. Wu, C.-L. Lee, Y. Hong, C.-H. Kuo, and M. H. Huang, "Plasmonic-enhanced polymer photovoltaic devices incorporating solution-processable metal nanoparticles," *Applied Physics Letters*, Vol. 95, No. 1, 013305, 2009.

124. Kim, Y.-H., S.-H. Lee, J. Noh, and S.-H. Han, "Performance and stability of electroluminescent device with self-assembled layers of poly(3,4-ethylenedioxythiophene)-poly(styrenesulfonate) and polyelectrolytes," *Thin Solid Films*, Vol. 510, No. 1–2, 305–310, 2006.

125. Van de Lagemaat, J., "Organic solar cells with carbon nanotubes replacing In$_2$O$_3$:Sn as the transparent electrode," *Applied Physics Letters*, Vol. 88, No. 23, 233503, 2006.

126. Wang, Y., S. W. Tong, X. F. Xu, B. Özyilmaz, and K. P. Loh, "Interface engineering of layer-by-layer stacked graphene anodes for high-performance organic solar cells," *Advanced Materials*, Vol. 23, No. 13, 1514–1518, 2011.

127. Schlatmann, A., "Indium contamination from the indium-tin-oxide electrode in polymer light-emitting diodes," *Applied Physics Letters*, Vol. 69, No. 12, 1764, 1996.

128. Chen, Z., B. Cotterell, W. Wang, E. Guenther, and S.-J. Chua, "A mechanical assessment of flexible optoelectronic devices," *Thin Solid Films*, Vol. 394, No. 1–2, 201–205, 2001.

129. Nair, R., P. Blake, A. Grigorenko, K. Novoselov, T. Booth, T. Stauber, N. Peres, and A. Geim, "Fine structure constant defines visual transparency of graphene," *Science*, Vol. 320, No. 5881, 1308–1308, 2008.

130. Bae, S., H. Kim, Y. Lee, X. Xu, J.-S. Park, Y. Zheng, J. Balakrishnan, T. Lei, H. Ri Kim, Y. I. Song, Y.-J. Kim, K. S. Kim, B. Ozyilmaz, J.-H. Ahn, B. H. Hong, and S. Iijima, "Roll-to-roll production of 30-inch graphene films for transparent electrodes," *Nature Nanotechnology*, Vol. 5, No. 8, 574–578, 2010.

131. Wöbkenberg, P. H., G. Eda, D. S. Leem, J. C. de Mello, D. D. C. Bradley, M. Chhowalla, and T. D. Anthopoulos, "Reduced graphene oxide electrodes for large area organic electronics," *Advanced Materials*, Vol. 23, No. 13, 1558–1562, 2011.

132. Han, T. H., Y. Lee, M. R. Choi, S. H. Woo, S. H. Bae, B. H. Hong, J. H. Ahn, and T. W. Lee, "Extremely efficient flexible organic light-emitting diodes with modified graphene anode," *Nature Photonics*, Vol. 6, No. 2, 105–110, 2012.

133. Gomez De Arco, L., Y. Zhang, C. W. Schlenker, K. Ryu, M. E. Thompson, and C. Zhou, "Continuous, highly flexible, and transparent graphene films by chemical vapor deposition for organic photovoltaics," *ACS Nano*, Vol. 4, No. 5, 2865–2873, 2010.

134. Lee, S., J. S. Yeo, Y. Ji, C. Cho, D. Y. Kim, S. I. Na, B. H. Lee, and T. Lee, "Flexible organic solar cells composed of P3HT:PCBM using chemically doped graphene electrodes," *Nanotechnology*, Vol. 23, No. 34, 344013, 2012.

135. Kim, C. S., S. S. Lee, E. D. Gomez, J. B. Kim, and Y.-L. Loo, "Transient photovoltaic behavior of air-stable, inverted organic solar cells with solution-processed electron transport layer," *Applied Physics Letters*, Vol. 94, No. 11, 113302, 2009.

136. Chambon, S., A. Rivaton, J.-L. Gardette, and M. Firon, "Photo- and thermal degradation of MDMO-PPV:PCBM blends," *Solar Energy Materials and Solar Cells*, Vol. 91, No. 5, 394–398, 2007.

137. Tian, Y. and T. Tatsuma, "Mechanisms and applications of plasmon-induced charge separation at TiO_2 films loaded with gold nanoparticles," *Journal of the American Chemical Society*, Vol. 127, No. 20, 7632–7637, 2005.

138. Liu, Z., W. Hou, P. Pavaskar, M. Aykol, and S. B. Cronin, "Plasmon resonant enhancement of photocatalytic water splitting under visible illumination," *Nano Letters*, Vol. 11, No. 3, 1111–1116, 2011.

139. Devadas, M. S., K. Kwak, J.-W. Park, J.-H. Choi, C.-H. Jun, E. Sinn, G. Ramakrishna, and D. Lee, "Directional electron transfer in chromophore-labeled quantum-sized Au25 clusters: Au25 as an electron donor," *Journal of Physical Chemistry Letters*, Vol. 1, No. 9, 1497–1503, 2010.

140. Nishijima, Y., K. Ueno, Y. Yokota, K. Murakoshi, and H. Misawa, "Plasmon-assisted photocurrent generation from visible to near-infrared wavelength using a Au-nanorods/TiO_2 electrode," *Journal of Physical Chemistry Letters*, Vol. 1, No. 13, 2031–2036, 2010.

141. Furube, A., L. Du, K. Hara, R. Katoh, and M. Tachiya, "Ultrafast plasmon-induced electron transfer from gold nanodots into TiO_2 nanoparticles," *Journal of the American Chemical Society*, Vol. 129, No. 48, 14852–14853, 2007.